Wetting and drying of an inert wall by a fluid in a molecular-dynamics simulation

M. J. P. Nijmeijer, C. Bruin, and A. F. Bakker
Laboratorium voor Technische Natuurkunde, P.O. Box 5046, 2600 GA Delft, The Netherlands

J. M. J. van Leeuwen
Instituut Lorentz, P.O. Box 9506, 2300 RA Leiden, The Netherlands
(Received 11 June 1990)

The contact angle in a wall-fluid system can be obtained directly from a visual inspection of the liquid-vapor meniscus or it can be calculated from the solid-liquid, solid-vapor and liquid-vapor surface tensions. These routes were exploited in two previous simulations in which the wetting of a wall was studied. Both simulations showed the existence of a wetting and a drying transition with changing wall-fluid interaction, but the location of especially the drying transition was not consistent. It was suggested that the discrepancy was due to the use of a "live" wall, i.e., a wall in which the particles are not fixed at their lattice positions, in the measurements of the surface tensions. We have replaced the live wall by an inert wall and measured the surface tensions again, treating the wall as an external field now. The contact angles that are calculated from these measurements agree with the visual observations.

I. INTRODUCTION

A typical situation in which wetting phenomena are discussed is the situation of a fluid at liquid-vapor coexistence in contact with a wall. The extent to which the wall is wetted by the liquid is measured by the contact angle θ, which is defined as the angle between the wall and the interface between the liquid and vapor phase. The angle can vary between 0 and π. A contact angle equal to 0 means that the wall is preferably covered with liquid, the wall is called "completely wet." A contact angle of π means the opposite case: The wall is preferably covered with vapor and is called "completely dry." The intermediate cases $0<\theta<\pi/2$ and $\pi/2<\theta<\pi$ are called "partially wet" and "partially dry," respectively. The contact angle is related to the three surface tensions that act on the contact line—where the meniscus meets the wall—by Young's law[1]

$$\gamma_{sv}=\gamma_{sl}+\gamma_{lv}\cos\theta\ , \tag{1.1}$$

with γ_{sv}, γ_{sl}, and γ_{lv} the surface tensions of the solid-vapor, the solid-liquid, and the liquid-vapor interface, respectively. In case of a completely wet wall $\gamma_{sv}=\gamma_{sl}+\gamma_{lv}$, which means that a solid-vapor interface is unstable with respect to a solid-liquid plus a liquid-vapor interface: A liquid layer will always intrude between the wall and the vapor. In case of a partially wet wall, $\gamma_{sv}<\gamma_{sl}+\gamma_{lv}$, the wall would still preferably be covered with the liquid but the cost of the additional liquid-vapor interface prevents a liquid layer from intruding. Similarly, a vapor layer will intrude between the wall and the liquid if the wall is completely dry whereas the cost of the liquid-vapor interface prevents this intrusion in the partially dry state.

Surface tensions change with, e.g., temperature or strength of the solid-fluid interaction; so a transition from the partially dry to the completely dry or from the partially wet to the completely wet state is possible. These transitions are genuine phase transitions, call the "drying" and "wetting" transition and their nature and location have attracted much attention in recent years.

The contact angle can be measured in a system where the meniscus actually meets the wall such as in a capillary, partially filled with liquid. The angle with which the meniscus borders on the wall can be obtained from a visual inspection of such a system. Young's law gives a second route to this angle: It can be calculated from a measurement of the surface tensions. Both routes were exploited in a molecular-dynamics simulation by Saville[2] in a study of Young's law. Saville enclosed a liquid and a coexisting vapor phase between two parallel walls, represented as external potentials with a variable interaction strength. The meniscus was defined as a plane of constant density, between the liquid and the vapor density. By placing the liquid slab perpendicular to the walls, Saville obtained a meniscus that meets the wall, and thus he could measure the contact angle visually. With the slab parallel to the walls, he obtained a common geometry to measure surface tensions and from the latter, Saville calculated the contact angles. Unfortunately, the two routes did not agree upon the value of the angle.

The confrontation of a visually measured contact angle with a calculated one also appeared in the comparison of two other, closely related simulations,[3,4] the first one by Sikkenk *et al.*, the second by the present authors. The type of wall and fluid, the temperature, etc., were the same in both simulations. As in Saville's simulations, the liquid and vapor phase were enclosed between two parallel walls but in Sikkenk's and our simulations, the walls were formed by a lattice of solid particles which were allowed to oscillate around their lattice positions. Therefore, the walls represented a thermodynamic phase rather than an external potential. The wetting properties of the

system were varied by changing the interaction strength between the solid and the fluid. The liquid slab was placed parallel to the walls in the first series of simulations[3] and the contact angles were calculated from measurements of the surface tensions. Starting from the completely dry state and increasing the interaction strength, a drying transition and subsequently a wetting transition were encountered, both of first order. The location of the drying transition, however, was at variance with the behavior of the density profiles. Whereas the contact angles predicted a completely dry wall for a certain range of attractive strengths, it was observed in the same range that a liquid layer, placed between the walls, was eventually adsorbed at one of them. This spontaneous transition from a completely dry to a partially dry state indicated that the latter state was preferred by the system although the contact angles implied the reverse. Van Swol[5] remarked that the calculation of the solid-fluid surface tensions could be a source of errors. The presence of stress in a "live" wall (a wall in which the particles are not fixed at their lattice positions) could have influenced the measurement of these surface tensions and in this way have affected the contact angle, as discussed previously.[3,5]

This hypothesis was tested in the second series of simulations.[4] We placed the liquid slab perpendicular to the walls and measured the contact angle visually. Thus circumventing the calculation of a solid-fluid surface tension, we obtained once more a series of contact angles which showed a drying and a wetting transition under variation of the wall-fluid interaction. The location of the wetting transition was not too far from the result of the first experiment but the drying transition was strongly shifted. Fortunately, it was now located at a position consistent with the behavior of the density profiles in the previous experiment.

The simulations of Sikkenk *et al.* initiated a density-functional calculation[6] of the wetting properties of the same wall-fluid system. With a nonlocal-density-functional combined with an "effective attractive interaction" and including the effects of substrate roughness, Velasco and Tarazona obtained a drying transition which was much closer to the result later on given by the second experiment. The wetting transition was again found to be in the region predicted by both simulations. Moreover, the calculation yielded a stronger first-order character in case of the wetting, than in case of the drying transition. The same difference in character had been observed in the visual measurements of the contact angle.

This paper is addressed to a third measurement of contact angles in a wall-fluid system which is the same as before apart from the representation of the wall. By using an inert wall, the difficulties of determining γ_{sl} and γ_{sv} should be diminished since such a wall is not subject to the effects of stress. Thereby, we hope to achieve consistency between surface-tension measurements on the one hand and direct measurements of the contact angle on the other hand. For that purpose, the conditions of the simulations were taken to be exactly the same as in the previous study[3] except for the treatment of the wall particles. Earlier simulations have indicated that the motion of the wall particles is not important for the behavior of the fluid.

II. DESCRIPTION OF THE SIMULATIONS

The system is the same as described before[3] apart from the fact that we fix the solid particles at the positions of a perfect lattice. The fluid particles move in a three-dimensional cubic box with periodic boundary conditions in all directions. The interaction potential ϕ_{AB} between a particle of type A and a particle of type B is of the Lennard-Jones 12-6 form,

$$\phi_{AB}(r)=4\varepsilon_{AB}[(\sigma_{AB}/r)^{12}-(\sigma_{AB}/r)^{6}] , \tag{2.1}$$

where A and B stand for either "solid" or "fluid," r denotes the distance between the particles, ε_{AB} sets the energy scale, and σ_{AB} the length scale of the potential. The interaction potentials are cut off at $2.5\sigma_{AB}$. The length of the box equals $L=29.1\sigma_{ff}$.

The solid substrate is built of three layers of a fcc lattice which requires 2904 solid particles. The layers form the (100) planes of the solid and are placed in the x-y plane of the computational box. The particles are fixed at their lattice positions and not allowed to move. The lattice spacing is determined by σ_{ss}, chosen as $\sigma_{ss}=0.847\sigma_{ff}$. This mismatch between σ_{ss} and σ_{ff} prevents a solidification of the first adsorbed fluid layers.

Due to the periodic boundary conditions, the fluid is enclosed in the z direction between the third and the first layer of the lattice. Therefore, there are two solid-fluid interfaces present in the computational box, one at each side of the wall. The system contains some 8500 fluid particles, an amount which ensures the presence of both a liquid and a vapor phase. The interaction strength ε_{sf} between solid and fluid is varied in the simulations and the wetting behavior is studied as a function of the relative interaction strength $\varepsilon_r=\varepsilon_{sf}/\varepsilon_{ff}$. The length scale σ_{sf} of this interaction is close to the mean of σ_{ss} and σ_{ff}: $\sigma_{sf}=0.941\sigma_{ff}$.[7] The temperature of the system is kept fixed at $T^*=k_BT/\varepsilon_{ff}=0.9$ which is in between the fluid's triple-point temperature $T_t^*\approx 0.7$ and the critical temperature $T_c^*\approx 1.26$. The reduced timestep $\Delta t^*=\Delta t\sqrt{\varepsilon_{ff}}/(\sigma_{ff}\sqrt{m_f})$ in the simulations was set to 0.01 where m_f denotes the mass of a fluid particle. The simulations were carried out on a special purpose computer: the Delft Molecular Dynamics Processor (DMDP).

We place a liquid slab in between and parallel to the two sides of the wall. It has been discussed before[3,8] that the following three cases can occur.

(i) For low values of ε_r, the liquid layer resides in the middle of the system and both sides of the wall are covered with vapor (see Fig. 1 which shows the reduced fluid density $n^*=n\sigma_{ff}^3$ as a function of $z^*=z/\sigma_{ff}$). This situation is the completely dry case and has a total surface tension of

$$\gamma_{\text{tot}}=2\gamma_{sv}+2\gamma_{lv} . \tag{2.2}$$

(ii) Increasing ε_r, the liquid is adsorbed at one side of the wall (see Fig. 2). This asymmetric configuration is the

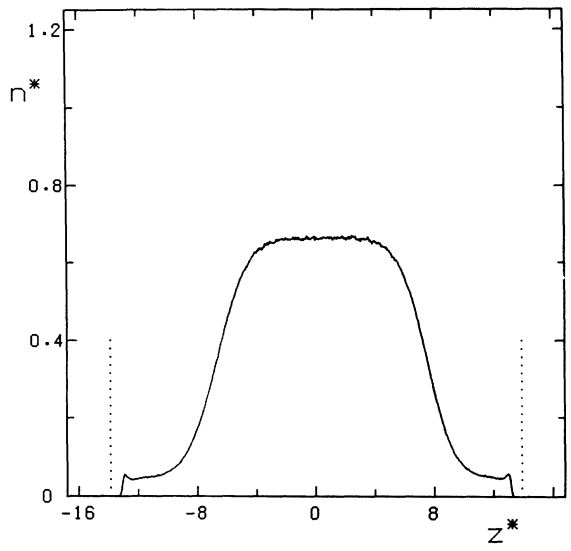

FIG. 1. Symmetric dry density profile at $\varepsilon_r=0.1$ obtained from an average over 3200 particle configurations generated in a run of 41 600 time steps. The dotted lines denote the positions of the outer layers of the wall. For convenience, the origin $z^*=0$ has been placed in the middle.

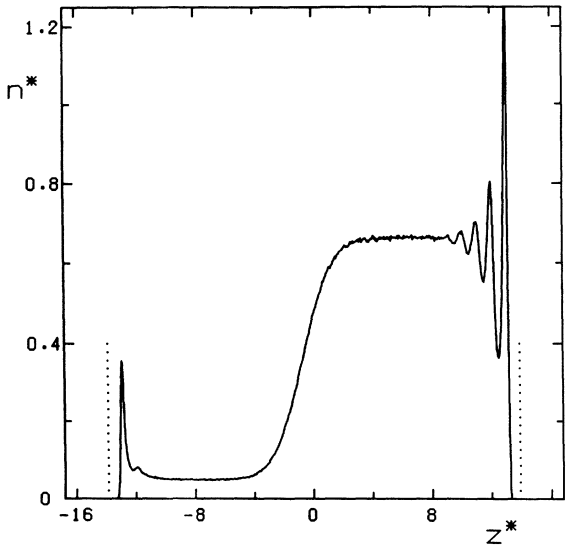

FIG. 2. Asymmetric density profile at $\varepsilon_r=0.5$ as averaged over 2400 particle configurations generated in 31 200 time steps. Further as Fig. 1.

partially dry or partially wet case. The total surface tension equals

$$\gamma_{\text{tot}}=\gamma_{sl}+\gamma_{lv}+\gamma_{sv} \ . \tag{2.3}$$

(iii) Finally, for large ε_r, both sides of the wall prefer to be covered with liquid (see Fig. 3). This is the completely wet case with a total surface tension

$$\gamma_{\text{tot}}=2\gamma_{sl}+2\gamma_{lv} \ . \tag{2.4}$$

Comparing the total surface tension of (i) and (ii), one recognizes that the transition from (i) to (ii) takes place at the drying point, i.e., $\theta=\pi$ in (1.1). The transition from (ii) to (iii) takes place at the wetting point $\theta=0$.

The solid-fluid surface tensions are measured differently from the previous procedure[3] where the wall was treated as a thermodynamic phase and the surface tension was measured in a way appropriate for an interface between two thermodynamic phases. In the present experiment, where the wall is represented by a rigid lattice of particles, one encounters the following difficulty in calculating the wall-fluid surface tensions. The standard way to measure the surface tensions runs via an integral over components of the pressure tensor which can be measured directly in a simulation. This expression is well known for a wall potential that has no lateral structure but it has not been extended to the case of a structured wall such as we encounter by placing individual wall particles on a lattice. This extension is nontrivial and presented in a separate paper.[9] It turns out that the expression for the wall-fluid surface tension of a structured wall is equal to the expression for a structureless wall. With the wall located at $z=0$ and the fluid at $z>0$, it is given by

$$\gamma_{sf}=\frac{1}{A}\int_A dx\,dy\int_0^\infty dz\left[p_N(\mathbf{r})-p_T(\mathbf{r})-n(\mathbf{r})z\frac{\partial}{\partial z}\phi^{\text{ext}}(\mathbf{r})\right] , \tag{2.5}$$

with A the area of the surface, p_N the component of the pressure tensor normal to the surface, p_T the component tangential to the surface, n the local density of the fluid, and ϕ^{ext} the external potential that forms the wall. In our case, the external potential is given by

$$\phi^{\text{ext}}(\mathbf{r})=\sum_l \phi_{sf}(|\mathbf{r}-\mathbf{a}_l|) \ , \tag{2.6}$$

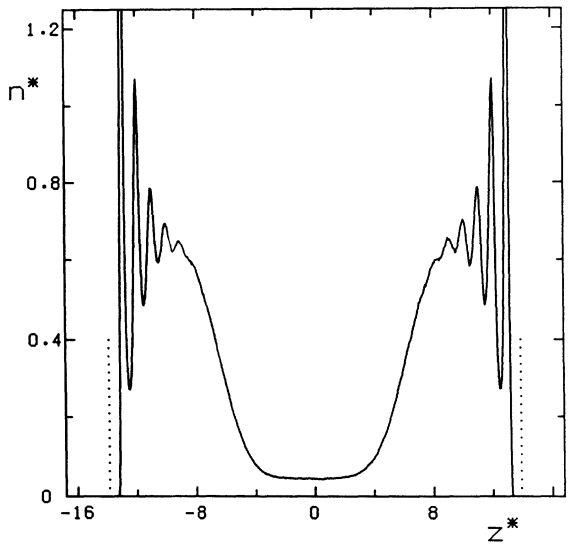

FIG. 3. Symmetric wet density profile at $\varepsilon_r=0.8$, further as Fig. 1.

where the sum is over all lattice positions $\mathbf{a}_l$. Note that the surface tension depends on the location of the origin $z=0$. A shift of this integration boundary with δz changes the surface tension with an amount $-p\delta z$, with p the pressure in the fluid. Since the pressure is the same in the liquid and the vapor phase, the arbitrariness has no influence on the difference $\gamma_{sv}-\gamma_{sl}$ which determines θ. We locate the boundary $z=0$ at the middle layer of the wall which is at equal distance from the solid-fluid interface at the left hand and the solid-fluid interface at the right-hand side. The surface tension of the whole system reads in our case

$$\gamma_{\rm tot}=\frac{1}{L^2}\int_{-L/2}^{L/2} dx\,dy\,dz\left[p_N(\mathbf{r})-p_T(\mathbf{r})-n(\mathbf{r})z\frac{\partial}{\partial z}\phi^{\rm ext}(\mathbf{r})\right]. \tag{2.7}$$

Inserting the microscopic definition[10] of p_N and p_T, it reads

$$\gamma_{\rm tot}=\frac{1}{L^2}\left\langle\sum_{(i,j)}\frac{\frac{1}{2}(x_{ij}^2+y_{ij}^2)-z_{ij}^2}{r_{ij}}\phi'_{ff}(r_{ij})\right\rangle-\frac{1}{L^2}\left\langle\sum_i z_i\frac{\partial}{\partial z}\phi^{\rm ext}(\mathbf{r}_i)\right\rangle, \tag{2.8}$$

with $\mathbf{r}_{ij}=\mathbf{r}_i-\mathbf{r}_j$, $\phi'_{ff}(r)$ the derivative of ϕ_{ff} with respect to r, and $\langle\ \rangle$ a canonical ensemble average. The first summation in (2.8) is over all pairs of fluid particles (i,j), the second summation over single fluid particles i. We measure a $p_N(z)$ and $p_T(z)$ defined by

$$p_N(z)=k_BTn(z)-\frac{1}{2L^2}\left\langle\sum_{\substack{i,j\\ i\neq j}}\frac{z_{ij}^2}{r_{ij}}\phi'_{ff}(r_{ij})\delta(z-z_i)\right\rangle, \tag{2.9}$$

$$p_T(z)=k_BTn(z)-\frac{1}{2L^2}\left\langle\sum_{\substack{i,j\\ i\neq j}}\frac{\frac{1}{2}(x_{ij}^2+y_{ij}^2)}{r_{ij}}\times\phi'_{ff}(r_{ij})\delta(z-z_i)\right\rangle, \tag{2.10}$$

with $n(z)$ the density $n(\mathbf{r})$ averaged over the x-y plane. One easily verifies that the substitution of (2.9) and (2.10) in (2.7) gives (2.8). The definitions (2.9) and (2.10) do not strictly conform to the general definition of Scnofield and Henderson[10] but this modification does not affect the surface tensions. A strict computation of the tensor according to their scheme would require a much more involved calculation. Considering, e.g., p_N, the contribution of a pair of particles (i,j) to the integral over p_N is given by $z_{ij}^2\phi'_{ff}(r_{ij})/r_{ij}$ as can be seen from (2.9). We have attributed half of this contribution to the z coordinate of particle i and half of the contribution to the z coordinate of particle j to obtain a local p_N. According to the general definition,[10] one should draw a contour between particles i and j and distribute the contribution of the pair over the contour in a well-specified manner. Different choices of contour correspond to different microscopic definitions of p_N. The spatial distribution of the contribution of the pair (i,j), however, is irrelevant for the integral over p_N.

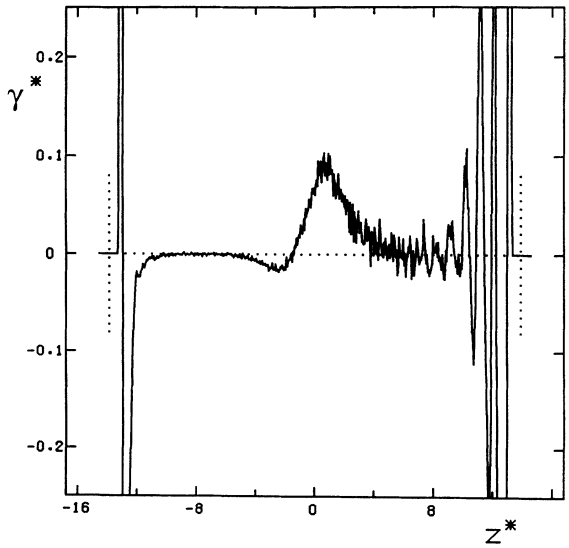

FIG. 4. "Surface-tension density" profile at $\varepsilon_r=0.5$ as averaged over 2400 particle configurations generated in 31 200 time steps. Further as Fig. 1. The reduced surface-tension density $\gamma^*(z)$ is defined as $\gamma^*(z)=\gamma(z)\sigma_{ff}^2/\varepsilon_{ff}$.

In other words, the integral over p_N is independent of its microscopic definition.

Since the integrand in (2.7) vanishes in a bulk phase where p_N and p_T both become equal to the pressure p and $\phi^{\rm ext}$ vanishes, the integral consists of a number of separate contributions, one from each interface in the system. This is clearly seen in Fig. 4 which shows the "surface tension density" $\gamma(z)$,

$$\gamma(z)=p_N(z)-p_T(z)-\frac{1}{L^2}\int_{-L/2}^{L/2} dx\,dy\,n(\mathbf{r})z\frac{\partial}{\partial z}\phi^{\rm ext}(\mathbf{r}), \tag{2.11}$$

of the asymmetric system of Fig. 2. The contribution of an individual interface is the interface's surface tension which is therefore obtained by restricting the integration over z in (2.7) to an integration over the surface alone.

III. RESULTS

As before, we simulated a series of asymmetric systems and symmetric dry and wet systems at various ε_r. A symmetric dry starting configuration at $\varepsilon_r=0.1$ was obtained by melting a strip of fluid particles, placed between the walls on a lattice with approximately the appropriate liquid density. An asymmetric starting configuration was obtained by choosing $\varepsilon_r=0.5$ whereupon the same initial strip was adsorbed at one of the sides of the wall during the melting process. A symmetric wet starting configuration resulted from the use of two strips, each one placed near one of the sides of the wall with $\varepsilon_r=0.8$. Systems at different ε_r were obtained by changing ε_r. A newly formed system was equilibrated for approximately 15 600 time steps before the measurements started. This equilibration time was sufficient to stabilize the particle

TABLE I. Reduced surface tensions of the liquid-vapor, solid-liquid, and solid-vapor interface, reduced total surface tension and the cosine of the contact angle in the asymmetric systems. The figures between parentheses denote the uncertainty (one standard deviation) in the last or last two digits. The reported γ_{sv}^* at $\varepsilon_r=0.7$ and 0.8 are the surface tensions of the metastable solid-vapor interfaces encountered in the asymmetric systems whereas one has $\gamma_{sv}^*=\gamma_{sl}^*+\gamma_{lv}^*$ in equilibrium since the wall is completely wet. The $\cos\theta$ of this metastable branch are larger than 1. Most results are obtained from an average over 32 000 configurations.

ε_r	γ_{lv}^*	γ_{sl}^*	γ_{sv}^*	γ_{tot}^*	$\cos\theta$
0.2	0.240(3)	0.263(7)	0.0298(7)	0.533(6)	−1.04(3)
0.3	0.219(7)	0.207(10)	0.0177(8)	0.444(15)	−0.84(5)
0.4	0.207(11)	0.101(8)	−0.0067(6)	0.302(16)	−0.48(4)
0.5	0.234(10)	−0.066(11)	−0.0400(16)	0.128(18)	0.12(5)
0.6	0.241(15)	−0.280(10)	−0.0990(26)	−0.138(20)	0.80(3)
0.7	0.214(11)	−0.541(7)	−0.1653(43)	−0.492(10)	1.67(3)
0.8	0.223(9)	−0.827(14)	−0.2747(45)	−0.879(16)	2.45(6)

density profile, the energy of the system, and other quantities in most cases. The particle density and surface-tension density profiles were sampled each 13th or 15th timestep until an average over some 3200 configurations was obtained. Error bars in the data denote the standard deviation as calculated from subaverages over 400 configurations.

The properties of the bulk liquid and bulk vapor phase and the properties of the liquid-vapor interface should be independent of ε_r. It has been verified that this independence holds for the reduced bulk densities n_l^* and n_v^* and the reduced liquid-vapor surface tension γ_{lv}^* where the latter is listed in Table I. These quantities fluctuate with varying ε_r but show no systematic dependence. Averaged over all ε_r, their mean values are $n_l^*=0.6640\pm0.0006$, $n_v^*=0.0456\pm0.0006$, and $\gamma_{lv}^*=0.225\pm0.005$, which corresponds with results obtained in a simulation[11] of a free liquid-vapor interface. Another check on the influence of ε_r is a measurement of the pressure in the system which should also be unaffected by ε_r. The pressure p can be calculated from[9]

$$p=\frac{1}{L^3}\int_{-L/2}^{L/2} dx\,dy\,dz\left[p_N(z)-n(\mathbf{r})z\frac{\partial}{\partial z}\phi^{\text{ext}}(\mathbf{r})\right]. \quad (3.1)$$

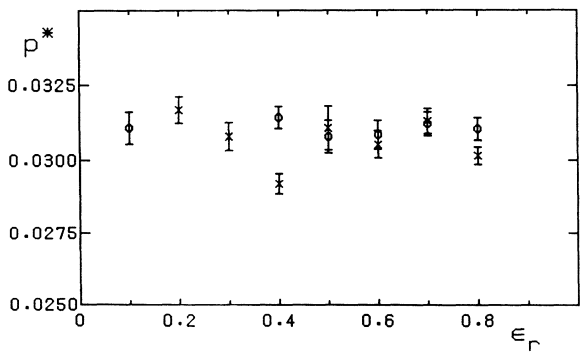

FIG. 5. Reduced pressure $p^*=p\sigma_{ff}^3/\varepsilon_{ff}$ as a function of ε_r. Circles denote the symmetric systems, crosses the asymmetric systems.

The result is plotted in Fig. 5 which shows a pressure that does not vary systematically with ε_r but fluctuates around an average value of $p^*=0.0308\pm0.0002$.

The completely dry state with the liquid slab in the middle of the system remains stable at $\varepsilon_r=0.1$ (see Fig. 1). Increasing ε_r to 0.2, one observes a transition to the asymmetric system of Fig. 6, the liquid layer being adsorbed at one of the sides of the wall. Before the state of Fig. 6 was obtained, the liquid slab, which was initially in the middle of the system, had first collided with the wall at the right whereupon it reflected back and was adsorbed at the left wall. The whole transition from a symmetric dry to the asymmetric system took about 60 000 time steps. The liquid layer remained adsorbed at the left side of the wall during the 57 000 time steps we followed it. The precise location of the symmetric-asymmetric transition is hard to tell since it is difficult to determine whether the solid-liquid interface one obtains at $\varepsilon_r=0.2$

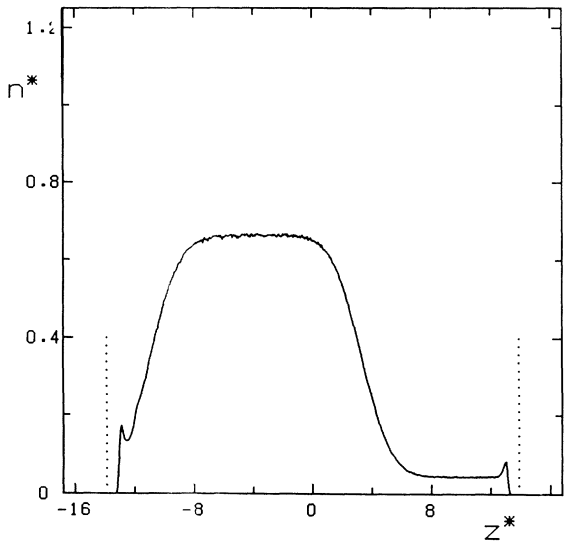

FIG. 6. Asymmetric density profile at $\varepsilon_r=0.2$, further as Fig. 1.

is indeed a stable solid-liquid interface or should be regarded as a metastable state in which the system is easily trapped due to the limited space between the walls while the completely dry state is the true equilibrium state. The state at $\varepsilon_r = 0.3$ is far less controversial. Starting with a symmetric dry system, one obtains an asymmetric system with a solid-liquid interface which clearly differs from the solid-vapor interface (cf. Fig. 7). The transition from a symmetric dry to an asymmetric system took about 30 000 time steps in the case $\varepsilon_r = 0.3$.

If we start with an asymmetric system at $\varepsilon_r > 0.2$ and lower ε_r, we observe the inverse transition. At $\varepsilon_r = 0.2$, the asymmetric system evolves again to a system similar to the one of Fig. 6. Decreasing ε_r to 0.1, we obtain a system with two solid-vapor interfaces although even in this case, the liquid phase remains near the wall it just detached from and stays slightly off center during at least 60 000 time steps.

The behavior of the density profiles thus shows the existence of a drying transition at $\varepsilon_r \approx 0.2$. We cannot observe any hysteresis in the location of the transition which indicates that it is possibly second, at least not strongly first order. The situation is quite different at the wetting transition. If we start with an asymmetric configuration and increase ε_r, we never observe a transition to a symmetric wet state, not even at $\varepsilon_r > 1$ which is well above the wetting transition.[3,4] Conversely, if we start with a symmetric wet state and decrease ε_r, we do not observe the transition to the asymmetric state, even not at ε_r as low as 0.4. This hysteresis in the density profiles reveals the presence of a first-order wetting transition but prevents an accurate location of the transition from the behavior of the profiles.

The second route to the location of the transitions is the measurement of the total surface tension in the various systems, the results of which are shown in Fig. 8 and

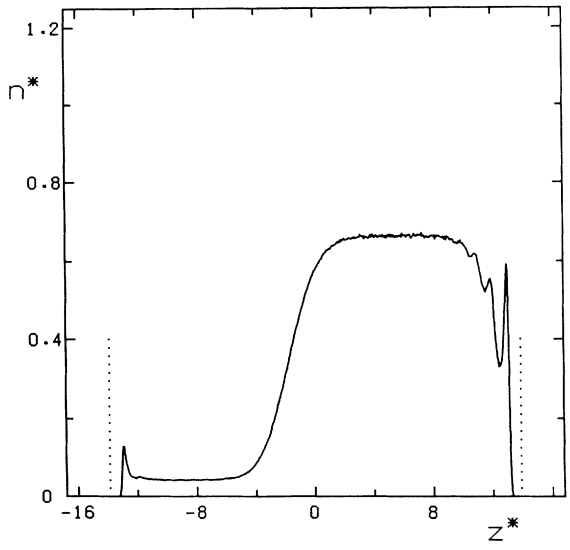

FIG. 7. Asymmetric density profile at $\varepsilon_r = 0.3$, further as Fig. 1.

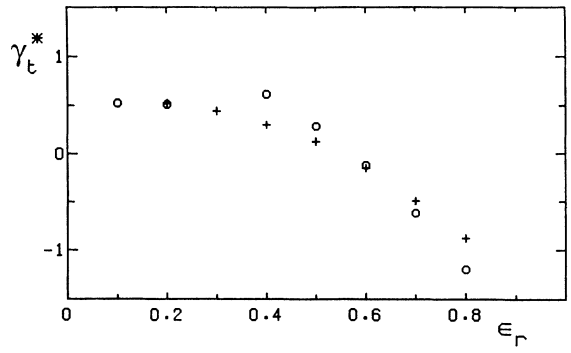

FIG. 8. Reduced total surface tension $\gamma^*_{\rm tot}$ as a function of ε_r. Circles denote the symmetric systems, crosses the asymmetric ones. The symmetric value at $\varepsilon_r = 0.2$ is constructed (see text). The experimental uncertainty is of the order of the symbol size.

listed in Tables I and II. The results are most clear at the wetting side where the strong hysteresis allows one to measure the surface tension of both the symmetric and the asymmetric state over a wide range of ε_r. The two curves intersect at $\varepsilon_r \approx 0.6$, below which the partially wet state is thermodynamically favorable, above which the completely wet state is preferred. The intersection point locates the wetting transition. One could argue that the total surface tension of the completely wet state is not well described by (2.4) since the liquid phases in these states are very small and the solid-liquid and liquid-vapor interfaces are not well separated. In that case, the location of the wetting transition as the intersection point in Fig. 8 would be incorrect. The effect of the finite size can be checked by calculating the total surface tension of a well-developed, symmetric state from (2.4) with γ_{sl} as obtained in an asymmetric system and $\gamma_{lv} = 0.225$. It turns out that $\gamma_{\rm tot}$ calculated in this way does not significantly differ from $\gamma_{\rm tot}$ as we measure it in the completely wet systems. Therefore, the restriction on the size of the symmetric wet systems turns out to have no significant effect on the location of the wetting transition.

There is no hysteresis at the drying side. At $\varepsilon_r = 0.2$, however, we can once more address the question of the

TABLE II. Reduced total surface tension in the symmetric dry system at $\varepsilon_r = 0.1$ and the symmetric wet systems from $\varepsilon_r = 0.4$ to 0.8. The figures between parentheses denote the uncertainty in the last or last two digits. Most results are obtained from an average over 32 000 configurations.

ε_r	$\gamma^*_{\rm tot}$
0.1	0.534(8)
0.4	0.612(8)
0.5	0.287(16)
0.6	−0.121(12)
0.7	−0.620(14)
0.8	−1.199(17)

stability of the system of Fig. 6 by comparing its total surface tension with the total surface tension of a completely dry system. The latter can be constructed from (2.2) with γ_{sv} measured in the asymmetric system of Fig. 6 and $\gamma_{lv}=0.225$. As shown in Fig. 8, the two surface tensions cannot be distinguished, showing that the solid-liquid interface of Fig. 6 has the same thermodynamic probability as a solid-vapor plus a liquid-vapor interface. The same comparison at $\varepsilon_r=0.3$ (not included in Fig. 8) shows that the total surface tension of the system of Fig. 7 is slightly below the constructed surface tension of a hypothetical, symmetric dry state. We stress once more that the total surface tension in Fig. 8 depends on the choice of origin $z=0$ but that the location of the intersection point is unaffected by this choice.

The last route to the wetting and drying transition is the calculation of the contact angles from the surface tensions. The angles are measured in the asymmetric systems which provide at the same time a solid-liquid and a solid-vapor interface while we used a fixed value of $\gamma_{lv}=0.225$ in the calculation of $\cos\theta$. Figure 9 shows the results together with the contact angles obtained from the visual measurements.[4] The wetting transition is given by $\cos\theta=1$, the drying transition by $\cos\theta=-1$. The location of these points is the same as given by the total surface tensions. The fact that the cosine as a function of ε_r crosses the line $\cos\theta=1$ with a finite slope once more supports the first-order character of the transition. A cosine larger than 1 shows that we have been measuring in a metastable state, a fact we also observed in the total surface tensions. If a curve would be drawn through the measured angles, its derivative with respect to ε_r would be small at the drying transition and should be zero if the transition were to be second order. It is difficult to tell whether the derivative is indeed zero or has a finite value but we can be sure that the drying transition has at most a weakly first-order character.

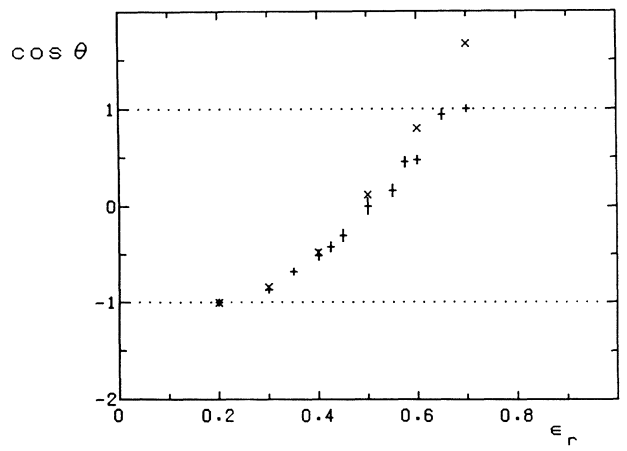

FIG. 9. Cosine of the contact angle vs ε_r. The crosses, ×, are the results as calculated from Young's law in these simulations, the errors are of the order of the symbol size (cf. Table I). The pluses, +, are the visual observations (Ref. 4), the length of the vertical bar gives the error.

The comparison of the calculated contact angles with the visual observations in Fig. 9 shows that they coincide but that the calculated angles can be determined with greater accuracy. The comparison is especially good near the drying transition while the calculated angles rise slightly more steeply near the wetting transition.

The visually measured angles differ marginally from the angles presented in the original paper.[4] The angles were obtained by fitting a circle to the liquid-vapor meniscus, a fit which was performed manually in the original work but which we have done presently numerically to exclude the possibility of uncontrolled errors which is inherent to a manual procedure. The numerical method, a least-squares fit, gives angles that vary a little bit smoother with ε_r but does not shift the curve as a whole. In particular, our estimates[4] of the position of the wetting and drying transition are not altered.

IV. CONCLUSIONS

We have examined the wetting properties of a wall-fluid system in a simulation very similar to the one performed by Sikkenk *et al.* but with the "live" wall replaced by an inert wall. Of the three routes to the location of the wetting and drying transition, only the behavior of the density profiles is the same as reported previously.[3] The other two routes involve the measurement of the solid-fluid surface tension, a measurement that is difficult with a live wall which can support stress. We have shown that the replacement of the live by an inert wall removes the inconsistency near the drying transition between the contact angles and the behavior of the profiles.[3] In the inert case, the three routes all agree on a location of this transition at $\varepsilon_d=0.20\pm0.05$, to be compared with the estimate[3] of $\varepsilon_d=0.54\pm0.03$. The drying transition we observe is weakly first or second order. There occurs a relatively smaller shift in the location of the wetting transition. This location cannot be obtained with any accuracy from the behavior of the density profiles but it appears very clearly in the data of the total surface tension and the contact angle. From these two routes, we estimate a strongly first-order wetting transition to occur at $\varepsilon_w=0.62\pm0.01$, compared with $\varepsilon_w=0.78\pm0.03$ as reported in the previous reference.[3] Part of these differences could be ascribed to the difference in type of wall but we expect that the relatively small oscillations of the wall particles around their equilibrium positions have little effect on the location of the transitions.

Moreover, our contact angle measurements agree with the visual measurements.[4] Those simulations gave estimates of $\varepsilon_d=0.24\pm0.04$ and $\varepsilon_w=0.68\pm0.03$, which coincide with the present measurements. The comparison could again be invalidated by the difference in type of wall and, additionally, by the curvature of the liquid-vapor interface that appears in the visual measurements. The curvature was reported to affect the state of the liquid and vapor phase, and therefore it influences γ_{sv}, γ_{sl}, and γ_{lv} which determine $\cos\theta$. However, from the agreement between the two ways to measure $\cos\theta$, we conclude that the effects of the freezing in of the wall and

the curvature are small. The two simulations also provide an explicit demonstration of Young's law which so far has escaped fluid simulations.

From the results of these simulations, there emerges a consistent picture of the wetting behavior of this particular wall-fluid system. The density functional calculation[6] is in line with this picture. The calculation predicts for the structured wall case, which is closest to the situation in the present simulation, a drying transition at $\varepsilon_d = 0.15$ followed by a wetting transition at $\varepsilon_w = 0.75$ and, moreover, it exhibits the difference in character between the two transitions.

Interestingly, a detailed study of the drying transition by Henderson and van Swol,[12] including both a density-functional calculation and a simulation, gave a different idea of this transition. They studied a square-well fluid in contact with a square-well wall and drove the transition in the same way as in our simulations: by changing the wall-fluid interaction strength while keeping the fluid at a fixed temperature. In their case, the density-functional calculation predicts a continuous transition while the simulations show a strongly first-order transition. Henderson and van Swol conclude that the apparent first-order nature of the drying transition is induced by collective, capillary wave-type fluctuations since these are not properly included in the density-functional calculations but do appear in the simulations. Whether their results are specific for a square-well system and do not hold for a system with truncated Lennard-Jones interactions, is a point of debate.

ACKNOWLEDGMENTS

We are indebted to F. Lange for assisting with the simulations and acknowledge the contribution of A. B. van Woerkom, who wrote the assembly programs to measure the pressure tensor. The numerical fits to the menisci of our previous work[4] were performed by E. Hirshowitz. Part of this research was supported by the "Stichting voor Fundamenteel Onderzoek der Materie" (FOM), which is financially supported by the "Nederlandse Organisatie voor Wetenschappelijk Onderzoek" (NWO).

[1]See, e.g., S. Dietrich, in *Phase Transitions and Critical Phenomena*, edited by C. Domb and J. Lebowitz (Academic, London, 1988), Vol. 12.

[2]G. Saville, J. Chem. Soc. Faraday Trans. **12**, 1122 (1977).

[3]J. H. Sikkenk, J. O. Indekeu, J. M. J. van Leeuwen, E. O. Vossnack, and A. F. Bakker, J. Stat. Phys. **52**, 23 (1988).

[4]M. J. P. Nijmeijer, C. Bruin, A. F. Bakker, and J. M. J. van Leeuwen, Physica A **160**, 166 (1989).

[5]F. van Swol, Phys. Rev. Lett. **60**, 239 (1988).

[6]A. Velasco and P. Tarazona, J. Chem. Phys. **91**, 7916 (1989).

[7]Erroneously, σ_{sf} was mentioned to be $0.912\sigma_{ff}$ previously (Refs. 3, 4, and 8) while those simulations were also carried out with $\sigma_{sf} = 0.941\sigma_{ff}$.

[8]J. M. J. van Leeuwen, M. J. P. Nijmeijer, and C. Bruin, Phys. Scr. **T25**, 256 (1989).

[9]M. J. P. Nijmeijer and J. M. J. van Leeuwen, J. Phys. A (to be published).

[10]D. Schofield and J. R. Henderson, Proc. R. Soc. London A **379**, 231 (1982).

[11]M. J. P. Nijmeijer, A. F. Bakker, C. Bruin, and J. H. Sikkenk, J. Chem. Phys. **89**, 3789 (1988).

[12]J. R. Henderson and F. van Swol, J. Phys. Cond. Matt. **2**, 4537 (1990).